Environmental Science and Pollution Research (2018) 25:27059–27073
https://doi.org/10.1007/s11356-018-2594-x

RESEARCH ARTICLE

Performance of ceria/iron oxide nano-composites based on chitosan as an effective adsorbent for removal of Cr(VI) and Co(II) ions from aqueous systems

Morshed Farokhi [1] · Arsalan Parvareh [1,2] · Mostafa Keshavarz Moraveji [1,3]

Received: 4 April 2018 / Accepted: 18 June 2018 / Published online: 17 July 2018

Abstract

A novel chitosan/ceria/iron oxide (CS/ceria/Fe_3O_4) nano-composite adsorbent was synthesized for removal of Cr(VI) and Co(II) ions from aqueous systems in a batch system. The adsorbents were characterized by field emission scanning electron microscopy (FESEM), Fourier transform infrared spectroscopy (FTIR), X-ray diffraction (XRD), transmission electron microscopy (TEM), thermal gravimetric analysis (TGA), and Brunauer- Emmett-Teller (BET) analyses. The behavior of swelling kinetics was also studied. The effect of several adsorption parameters including CeO_2 and Fe_3O_4 contents, initial pH, contact time, initial Cr(VI) and Co(II) concentration, and temperature on the adsorption capacity was studied. The double exponential model revealed a better fit with the kinetic data of Cr(VI) and Co(II) ions. The Cr(VI) and Co(II) adsorption process well fitted the Langmuir model. The maximum adsorption capacities estimated from Langmuir isotherm model were 315.4 and 260.6 mg/g for Cr(VI) and Co(II) ions, respectively. Also, thermodynamic parameters were used to distinguish the nature of Cr(VI) and Co(II) adsorption. The reusability of CS/ceria/Fe_3O_4 nano-composite was evaluated with stripping agents of 0.1 M NaOH and 0.1 M HNO_3. Finally, the evaluation of Cr(VI)-Co(II) coexisting system confirmed that the presence of Co(II) ions played an inhibitor role on the Cr(VI) adsorption.

Keywords Adsorption · Chitosan/ceria/iron oxide · Nano-composite · Reusability · Swelling

Introduction

The aqueous environments have been contaminated significantly by poisonous heavy metals such as cobalt (Co(II)) and chromium (Cr(VI)) ions because these heavy metal ions are applied in paint manufacture, mining, petroleum refining, printing industries, and other industrial processes (Ahmadpour et al. 2009; Li et al. 2015; Zhong et al. 2013). Even at low concentration, the release of heavy metals into the streams increases the risk of liver and skin cancers and also severe diarrhea which is a serious threat to human health. These heavy metal ions have high poisonousness and lead to bioaccumulation through the food chain (Chen et al. 2011; Sirk et al. 2009). Various purification methods such as precipitation (Becker et al. 2012), electrochemical treatment (Mirbagheri and Hosseini 2005), membrane process (Kim et al. 2017), solvent extraction (Coll et al. 2012), ion exchange (Bai and Bartkiewicz 2009), flotation (Polat and Erdogan 2007), and adsorption processes (Prakash et al. 2016; Prakash et al. 2013; Prakash et al. 2012; Tehrani et al. 2017) have been developed for wastewater treatment. Among these technologies, adsorption is preferred for heavy metal removal at low concentration because of its simplicity, high efficiency, and cost-effectiveness (Petrella et al. 2018). In general, chromium exists as an anion, i.e., $HCrO_4^-$ and $Cr_2O_7^{2-}$, while cobalt exists as cation in aqueous solution (Ahmadpour et al. 2009; Shen et al. 2012). Therefore, the adsorbents designed by effective methods are needed to remove the anions and cations from aqueous systems. Various nano-adsorbents such as iron

Responsible editor: Philippe Garrigues

✉ Mostafa Keshavarz Moraveji
moraveji@aut.ac.ir

[1] Department of Chemical Engineering, Borujerd Branch, Islamic Azad University, Borujerd, Iran

[2] Chemical Engineering and Petroleum Faculty, Razi University, Kermanshah, Iran

[3] Department of Chemical Engineering, Amirkabir University of Technology (Tehran Polytechnic), 242 Hafez Avenue, Tehran 15875-4413, Iran

oxide and ceria nanoparticles have been applied to remove the toxic metal ions from water systems due to the meaningful advantages including higher surface area, higher electric charge, and more available active sites compared to the particles in micro scale (Liu et al. 2008; Recillas et al. 2010; Zhang et al. 2014). However, the recycling of metal oxide nanoparticles from water is very difficult after adsorption process. Also, the instability and agglomeration of nanoparticles are drawbacks of nanoparticles in the water treatment field owing to the several interactions and van der Waals forces (Zhang et al. 2014; Zhu et al. 2017). To suppress nanoparticle limitations, recently, the attention of researchers has focused on the loading of metal oxide nanoparticles on the polymeric solids such as chitosan in adsorption process (Sureshkumar et al. 2016; Wang et al. 2016). Chitosan is a biodegradable and non-toxic polymer which possesses hydroxyl and amine functional groups reacting with metal ions and improves the adsorption properties (Bhatnagar and Sillanpää 2009; Sureshkumar et al. 2016; Wang et al. 2016). The effect of ceria/Fe_3O_4 nano-composites based on chitosan has so far not been evaluated in Cr(VI) and Co(II) adsorption.

In the present research, a novel chitosan/ceria/Fe_3O_4 nano-composite was evaluated for the removal of both Cr(VI) and Co(II) ions from water systems. The prepared nano-composite adsorbents were characterized by field emission scanning electron microscopy (FESEM), Fourier transform infrared spectroscopy (FTIR), X-ray diffraction (XRD), transmission electron microscopy (TEM), Brunauer-Emmett-Teller (BET), and thermal gravimetric analysis (TGA) analyses. The behavior of swelling kinetics was used for the stability of chitosan/ceria/Fe_3O_4 nano-composite in aqueous solution. In a batch single system, the adsorption capacity was considered as a function of CeO_2 and Fe_3O_4 contents, contact time, pH, temperature, and initial Cr(VI) and Co(II) concentration. Also, adsorption kinetics, isotherms, and thermodynamic investigations were employed to analyze the experimental data. The reusability of chitosan/ceria/Fe_3O_4 adsorbent was examined after four cycles of adsorption-desorption. Furthermore, the adsorption of metal ions in the Cr(VI)-Co(II) coexisting system (binary system) was evaluated at two different pH 3.0 and 8.0.

Experimental sections

Materials

Chitosan (95%, molecular weight 200 kDa), oxalic acid, urea, acetic acid, ferrous sulfate heptahydrate ($FeSO_4{\cdot}7H_2O$), and ferric chloride hexahydrate ($FeCl_3{\cdot}6H_2O$) were prepared by Merck (Germany) and cerium nitrate hexahydrate ($Ce(NO_3)_3{\cdot}6H_2O$) was purchased from Fluka with high purity. The glacial acetic acid (Aldrich) was used as a solvent for chitosan. To prepare stock solution of Cr(VI) and Co(II) ions, the specified amount of potassium dichromate and cobalt nitrate hexahydrate were used. All materials were used as received. Also, deionized water was utilized in the synthesis of nano-composites and adsorption experiments.

Synthesis of ceria nanoparticles

The ceria nanoparticles were synthesized by a co-precipitation method (Sun et al. 2016). Firstly, 14.33 g of $Ce(NO_3)_3{\cdot}6H_2O$, 5.94 g of oxalic acid, and 5.96 g of urea were dissolved in distinct amount of deionized water to prepare the 0.165 M of $Ce(NO_3)_3{\cdot}6H_2O$, 0.330 M of oxalic acid, and 0.495 M of urea, respectively. Then, a 1 M solution was attained. After that, the solution pH was adjusted to 5.0 by using 36% acetic acid. Then, the volume of solution reached to 200 ml with deionized water under stirring for 120 min. The final solution was centrifuged at 3000 rpm for 20 min. Then, precipitate obtained from the centrifuge was washed with ethanol and deionized water three times to remove the excess materials. Finally, the final precipitate was converted to CeO_2 nanoparticles through calcination at 400 °C for 3 h (Sun et al. 2016).

Synthesis of Fe_3O_4 nanoparticles

Magnetite nanoparticles (Fe_3O_4) were also synthesized by a co-precipitation method (Sureshkumar et al. 2016). Firstly, 30 ml of 0.75 M $FeCl_3{\cdot}6H_2O$ and 15 ml of 0.75 M $FeSO_4{\cdot}7H_2O$ were mixed into a 250-ml beaker under stirring for 15 min. After that, 10 ml of 30% NaOH was added to the precursor solution. After addition of NaOH, the solution turned into a black color. The resulting solution was stirred further (continued for 60 min) to provide uniform black solution (Sureshkumar et al. 2016) and centrifuged at 3000 rpm. Finally, the black precipitate separated by centrifuge was washed with deionized water and dried at 70 °C for 12 h.

Fabrication of chitosan/ceria/Fe_3O_4 nano-composite adsorbents

Firstly, 2.5 g of chitosan was added to 200 ml of acetic acid (1%) under stirring for 4 h to prepare the chitosan solution. Then, the solution pH was adjusted to 5.0. After that, different contents of ceria nanoparticles (0.0, 0.25, 0.50, 0.75, 1.0, 1.25, and 1.5 g) were dispersed in chitosan solution under stirring for 3 h to obtain a homogeneous solution (solution A). Finally, the solution A was filtrated and washed with ethanol and deionized water and dried at 60 °C for 48 h. The resulting samples were chitosan/ceria nano-composites. To prepare the primary solution of chitosan/ceria/Fe_3O_4 nano-composite, various amounts of iron oxide (0.4, 0.6, 0.8, 1.0, 1.2, and 1.4 g) were dispersed in chitosan/CeO_2 solution

(solution A) under stirring for 3 h to get solution B. The operations of filtration, washing, and drying were similar to those mentioned above.

Characterization of prepared samples and determination of pH_{pzc}

Thermal stability and decomposition of prepared chitosan, chitosan/ceria, and chitosan/ceria/Fe_3O_4 nano-composite adsorbents were studied by using a Mettler Toledo TGA-851 thermogravimetric analyzer (Mettler, Switzerland). The surface morphology of ceria, Fe_3O_4, and chitosan/ceria/Fe_3O_4 samples was investigated after gold coating using a FESEM technique (SIGMA VP-500 model, Zeiss). Also, the shape of nanoparticles was studied by TEM analysis (Zeiss-EM10C-100 KV model, Germany). The phase identification of the adsorbent samples was performed by XRD analysis (X'Pert PRO model, PANalytical) with a Cu K_α radiation in the 2θ range of 10–80°. The functional groups of nano-composites were determined using FTIR analysis (PerkinElmer, RXI model). The surface area, average pore volume, and average pore diameter of samples were determined by BET method (BELSORP model, Japan). Cr(VI) and Co(II) ion concentrations in aqueous solutions were identified using an inductivity coupled plasma spectrophotometer (PerkinElmer, Aanalys200). Also, the point of zero charge (pH_{pzc}) of chitosan/ceria/Fe_3O_4 nano-composite adsorbent was specified as follows. Firstly, 50 ml of 0.1 M NaCl solution was transferred to a series of flasks. The values of initial pH were adjusted from 1.0 to 7.0 by using 0.1 M NaOH and/or 0.1 MHCl solutions. After that, 0.1 g of nano-composite adsorbent was added to each flask and the resulting mixtures were shaken for 48 h. The final pH values of each solution were determined using a portable pH meter. Finally, pH_{final} values were plotted versus corresponding $pH_{initial}$ values. The pH_{pzc} of nano-composite was estimated from the intersection point of the resulting curve with $y = x$ (Abbasizadeh et al. 2013).

Swelling behavior of chitosan/ceria/Fe_3O_4 nano-composite adsorbent

The dry polymeric chitosan/ceria/Fe_3O_4 adsorbent was immersed in water at different times to reach the equilibrium swelling. The swelling ratio (SR) was calculated as follows (Kim et al. 2003):

$$\mathrm{SR} = \frac{W_t - W_\mathrm{d}}{W_\mathrm{d}} \tag{1}$$

where W_d is dry weight of polymeric adsorbent and W_t is the swollen polymeric adsorbent at time t.

Adsorption experiments

The adsorption of Cr(VI) and Co(II) ions onto the CS/ceria/Fe_3O_4 nano-composite adsorbent was investigated as a function of CeO_2 and Fe_3O_4 contents, pH, contact time, temperature, and initial Cr(VI) and Co(II) concentration. The batch adsorption experiments were carried out in the flasks containing 25 ml solutions by shaking at 150 rpm. To obtain the optimum contents of nanoparticles, the effect of ceria and Fe_3O_4 contents was considered on Cr(VI) and Co(II) adsorption at a temperature of 25 °C, contact time of 100 min, and initial concentration of 200 mg/l, with an adsorbent dose of 12.5 mg and pH 5.0. To consider the influence of pH, the adsorption experiments were carried out at 25 °C, contact time of 100 min, and initial concentration of 200 mg/l, with an adsorbent dose of 12.5 mg at the different pH values in the range of 3.0–9.0. The influence of contact time and initial Cr(VI) and Co(II) concentrations was studied in the range of 0–100 min and 30–500 mg/l, respectively, at 25 °C with an adsorbent dose of 12.5 mg and an optimum pH. The effect of temperature on Cr(VI) and Co(II) ion adsorption was studied in the range of 25–45 °C. Furthermore, the adsorption of metal ions in the Cr(VI)-Co(II) coexisting system were studied at 25 °C, contact time of 100 min with an adsorbent dose of 12.5 mg, and two different values of pH (3.0 and 8.0). The adsorption capacity of chitosan/ceria/Fe_3O_4 nano-composite adsorbents was determined by the following equation:

$$q_e = \frac{(C_0 - C_e)V}{m} \tag{2}$$

where q_e is the equilibrium adsorption capacity of chitosan/ceria/Fe_3O_4 nano-composite for Cr(VI) and Co(II) ions (mg/g), C_0 and C_e represent the initial and equilibrium concentrations of metal ions (mg/l), respectively, m is the amount of dry adsorbent used in adsorption process (g) and V is the volume of metal ion solution (L).

Regeneration of chitosan/ceria/Fe_3O_4 nano-composite adsorbent

The regeneration of the adsorbent is a key factor because of its economic impact on adsorption process. After adsorption experiments, the Cr(VI) and Co(II) ions loaded on the surface of chitosan/ceria/Fe_3O_4 nano-composite adsorbent were separated by using stripping agents including 0.1 M HNO_3 and 0.1 M NaOH. The spent adsorbent was transferred to desorption medium and shaken for 100 min at a temperature of 25 °C and an initial metal concentration of 200 mg/l. The metal ions (Cr(VI) and Co(II)) loaded on the adsorbent surface were migrated from the adsorbents to the medium of desorbing agent under mentioned conditions. The reusability of the CS/ceria/Fe_3O_4

nano-composite adsorbent was investigated for four cycles of adsorption-desorption.

Results and discussion

Adsorbent characterization

To characterize the size and shape of particles on a solid surface, FESEM technique was used. SEM result (Fig. 1a) revealed that the Fe_3O_4 nanoparticles synthesized by the co-precipitation method were uniformly distributed with spherical morphology and the size of nanoparticles was in nano scale (25–38 nm). FESEM analysis (Fig. 1b) proved the irregular structure of CeO_2 nanoparticles. As shown, the CeO_2 nanoparticles were well synthesized. High proportion of CeO_2 nanoparticles had a spherical shape and also their size was in the range of 33–69 nm. FESEM image of chitosan/ceria/Fe_3O_4 nano-composite is shown in Fig. 1c. As observed, the iron oxide and cerium oxide nanoparticles had been uniformly distributed on the chitosan surface with a spherical structure and high density. Moreover, TEM image of chitosan/Fe_3O_4/CeO_2 nano-composite (Fig. 1d) indicated that the surface of chitosan had been successfully coated with CeO_2 and Fe_3O_4 nanoparticles. TEM analysis confirmed the results of FESEM analysis. The spherical morphology and uniform distribution of nanoparticles were clearly observed and also average particle size of nanoparticles was 35 nm.

In order to identify the phase and structure of crystalline materials, XRD analysis was used. XRD patterns of Fe_3O_4, CeO_2 nanoparticles synthesized by the co-precipitation method, and chitosan/CeO_2/Fe_3O_4 nano-composite are shown in Fig. 2. The XRD pattern of Fe_3O_4 nanoparticles conformed to the Joint Committee on Powder Diffraction Standards (JCPDS) standard no. 65-3107 which is displayed in Fig. 2a. As shown, the position of (220), (311), (400), (511), and (440)

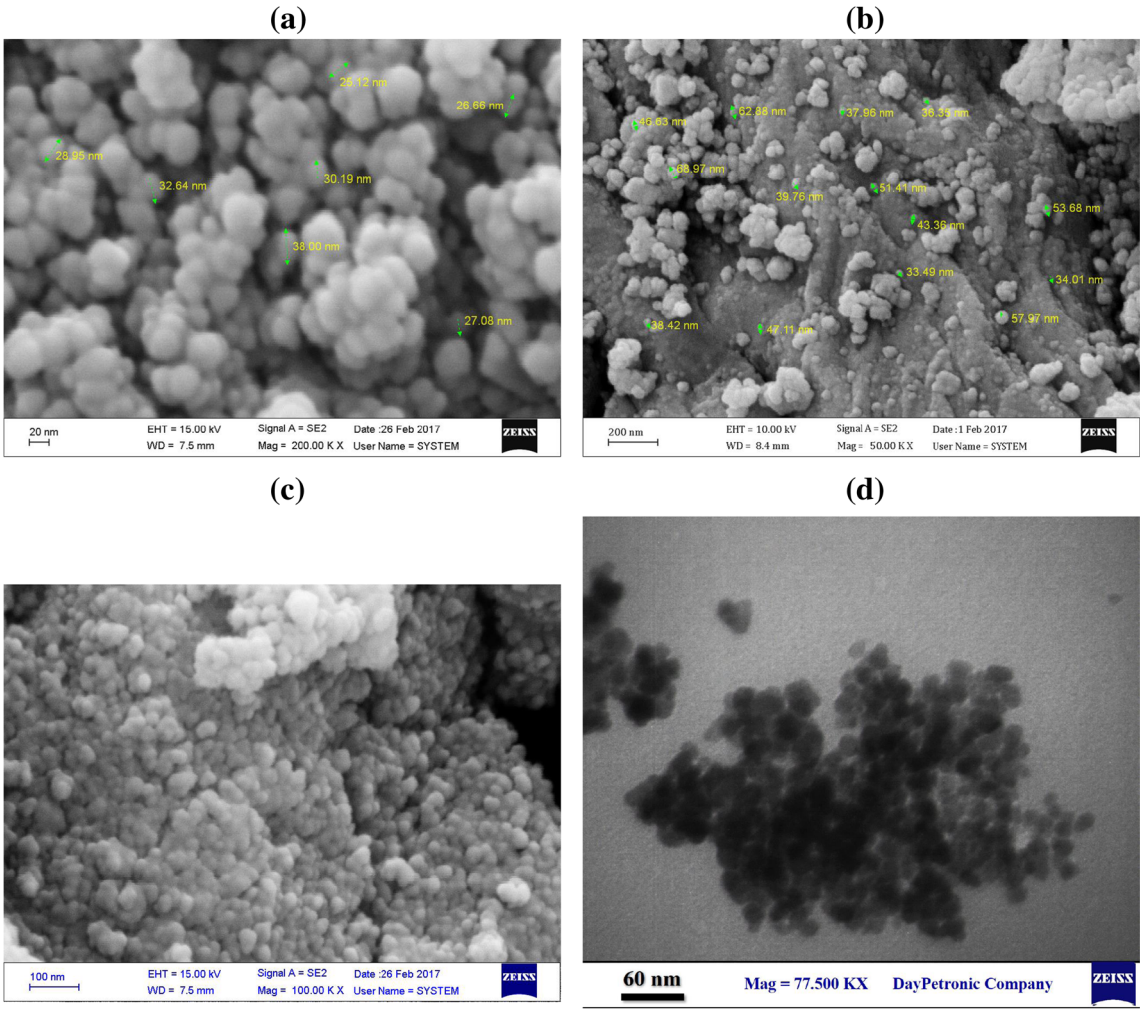

Fig. 1 FESEM images of **a** synthesized Fe_3O_4, **b** CeO_2 nanoparticles, **c** CS/ceria/Fe_3O_4, and **d** TEM images of CS/ceria/Fe_3O_4 nano-composite adsorbents

diffraction peaks matched well with those of the Fe_3O_4 nanoparticles. Similar XRD patterns were obtained by other researchers (Sureshkumar et al. 2016). Figure 2b indicates the XRD pattern of CeO_2 nanoparticles. As observed, the crystal surfaces of (111), (200), (220), (311), (222), (400), (331), and (420) corresponded to the CeO_2 phase based on JCPDS standard no. 34-0394 (Recillas et al. 2010). The XRD patterns confirmed the high purity of nanoparticles synthesized by the co-precipitation method because there were no excess peaks in the corresponding patterns. XRD pattern of CS/ceria/Fe_3O_4 nano-composite is illustrated in Fig. 2c. The corresponding diffraction peaks of ceria and Fe_3O_4 were observed which confirmed the presence of Fe_3O_4 and CeO_2 nanoparticles in the nano-composite structure. Comparison of all patterns is indicated in Fig. 2d. As shown, the full compliance of corresponding peaks in the chitosan/CeO_2/Fe_3O_4 nano-composite proved that the ceria and iron oxide crystalline structure had been successfully reserved with dispersion of nanoparticles on the surface of chitosan.

The BET surface area, average pore diameter, and total pore volume of chitosan/ceria and chitosan/ceria/Fe_3O_4 nano-composite with different contents of CeO_2 and Fe_3O_4 nanoparticles were estimated using the BET multipoint method under N_2 gas at temperature of 77 K. The results are given in Table 1. The results indicated that the S_{BET} and average total pore volume of chitosan/CeO_2 increased remarkably with the increase of CeO_2 contents from 0.25 to 1.0 g. This increase can be due to the presence of CeO_2 nanoparticles in the nano-composite structure. Further increase in CeO_2 contents (1.25 and 1.5 g) led to a decrease in the specific surface area of chitosan/CeO_2 nano-composite. The S_{BET} and average total pore volume of chitosan/CeO_2/Fe_3O_4 nano-composites increased with the increase of Fe_3O_4 contents up to 1.2 g. Further increase in Fe_3O_4 contents (1.4 g) resulted in a decrease in total surface area. The reduction of the S_{BET} and average total pore volume of nano-composites with high contents of CeO_2 (1.5 g) and Fe_3O_4 (1.4 g) can be due to the instability of nanoparticles leading to blockage of the pores

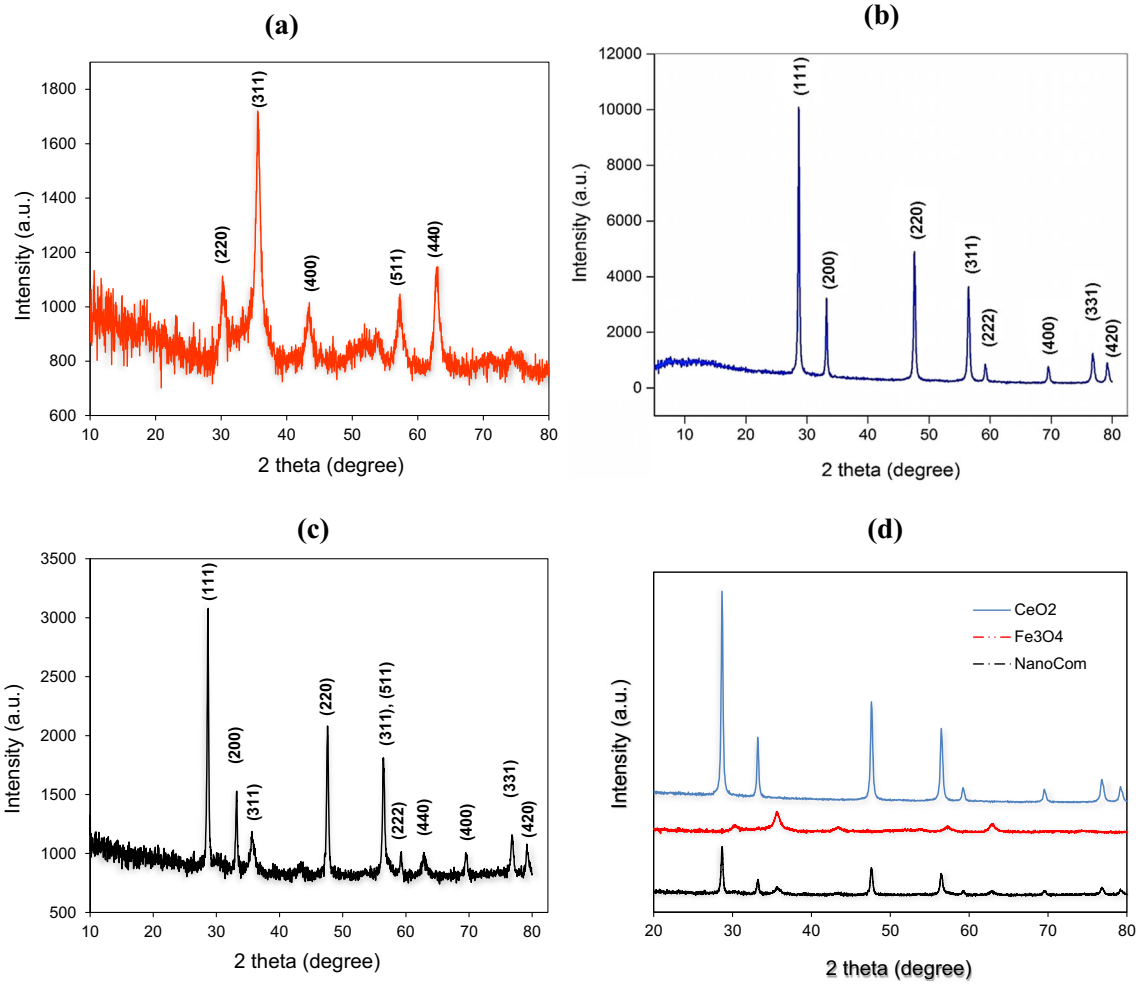

Fig. 2 XRD patterns of **a** Fe_3O_4, **b** CeO_2 nanoparticles, **c** CS/ceria/Fe_3O_4 nano-composite, and **d** the comparison of XRD patterns

Table 1 The S_{BET}, total pore volumes, and average diameters of CS/ceria and CS/ceria/Fe_3O_4 nano-composites

Sample	S_{BET} (m^2/g)	V_{total} (cm^3/g)	Average diameter (nm)
Chitosan/CeO_2 (0.25 g)	81.2	0.0447	2.451
Chitosan/CeO_2 (1.00 g)	100.5	0.0559	2.312
Chitosan/CeO_2 (1.50 g)	92.8	0.0503	2.396
Chitosan/CeO_2/Fe_3O_4 (0.4 g)	105.0	0.0582	2.302
Chitosan/CeO_2/Fe_3O_4 (1.2 g)	118.7	0.0657	2.214
Chitosan/CeO_2/Fe_3O_4 (1.4 g)	108.5	0.0603	2.283

of adsorbent by agglomeration of nanoparticles (Ray and Shipley 2015). Among the nano-composites, the highest surface area and average pore volume were found to be 118.7 m^2/g and 0.0603 cm^3/g, respectively, for chitosan/CeO_2/Fe_3O_4 with 1.0 g of CeO_2 and 1.2 g of Fe_3O_4 nanoparticles.

FTIR analysis was used to specify the functional groups of samples. The FTIR spectra of the pure chitosan and chitosan/CeO_2/Fe_3O_4 nano-composite adsorbents are indicated in Fig. 3a. As observed, the broad absorption band at 570–900 cm^{-1} was due to the stretching vibrations of Fe-O and Ce-O groups confirming the presence of Fe_3O_4 and CeO_2 nanoparticles in the nano-composite structure (Sureshkumar et al. 2016; Yari et al. 2015). The absorption peaks in the range of 1050–1150 cm^{-1} corresponded to the C-O stretching vibrations. The band at 1550–1640 cm^{-1} was assigned to the stretching vibrations of amide (N-H) groups. The absorption peak at 2925 cm^{-1} and absorption peaks at about 1050–1150 cm^{-1} corresponded to the C-H and C-O stretching vibrations, respectively. The absorption peak at 3430 cm^{-1} was attributed to the stretching vibrations of O-H groups.

The TGA curves for the pure chitosan, chitosan/ceria, and CS/ceria/Fe_3O_4 adsorbents are presented in Fig. 3b. Three degradation steps for pure chitosan were observed. It is shown that the first thermal decomposition of chitosan occurred in the temperature range of 40–200 °C. This mass loss can be due to the water evaporation in the nano-composite structure (Ferfera-Harrar and Dairi 2014; Taboada et al. 2009). The second and major step of weight loss occurred in the temperature range of 240–410 °C relating to the thermal degradation of the chitosan containing deacetylation (Taboada et al. 2009). The third step happened with further heating (410–800 °C) due to the breaking of chitosan backbone and degradation of chitosan byproducts. This degradation can be due to the pyrolitic and depolymerization processes (Taboada et al. 2009). For chitosan, CS/ceria, and CS/ceria/Fe_3O_4, total weight loss was found to be 94.0, 70.0, and 49.0%, respectively. The presence of inorganic CeO_2 and Fe_3O_4 nanoparticles in the nano-composite structure led to a higher thermal stability for CS/ceria and CS/ceria/Fe_3O_4 adsorbents compared to chitosan. The stability of inorganic material such as CeO_2 and Fe_3O_4 nanoparticles against temperature up to 800 °C was high. The similar behavior was observed by others; they showed that no significant weight loss observed ranging from room temperature to 800 °C (Cao et al. 2014).

Time-dependent swelling behavior of chitosan/ceria/Fe_3O_4 nano-composite adsorbent is indicated in Fig. 4a. As shown, the SR of nano-composite increased quickly within 720 min and then the curve leveled off, approximately. Finally, the equilibrium SR was found to be 2.52. In general, SR greater than one means that chitosan/ceria/Fe_3O_4 nano-composite is hydrophilic. It can be due to the surface hydroxyl groups of chitosan and nanoparticles. The swelling kinetics and water-transfer mechanism are important factors to explain the swelling properties due to the diffusion of water into the polymer and the swelling of the polymeric sample. There are different types of adsorption mechanisms of polymeric sample. The water penetration into the network of polymer, relaxation of polymer chains, and polymer structure stretch in the solution are the first, second, and third process, respectively. In order to interpret the mechanism of penetrating, the following equation was applied (Kim et al. 2003):

$$\frac{M_t}{M_\infty} = kt^n \tag{3}$$

where M_∞ and M_t are water contents adsorbed at equilibrium and time t, respectively; n represents the kinetic exponent which interprets the mode of penetrant transport and k is the swelling rate front factor. The values of k and n were estimated from intercept and slope of linear form of Eq. 3, respectively (Fig. 4b). When the penetrating diffusion rate is rate-limiting, a Fickian mechanism dominates ($n = 0.5$). When $0.5 < n < 1.0$, a distinctive non-Fickian mechanism happens during the swelling process and the solute transport is anomalous. When $n = 1.0$, the relaxation mechanism is rate-limiting. In this study, the results indicated that the swelling of chitosan/ceria/Fe_3O_4 nano-composite adsorbent obeyed from non-Fickian mechanism because n value was greater than 0.5 (0.635).

Effect of Fe_3O_4 and CeO_2 contents on Cr(VI) and Co(II) adsorption

The effect of CeO_2 and Fe_3O_4 nanoparticles on the structure of nano-composite adsorbent for the removal of Cr(VI) and Co(II) ions from aqueous system was studied at 25 °C, initial

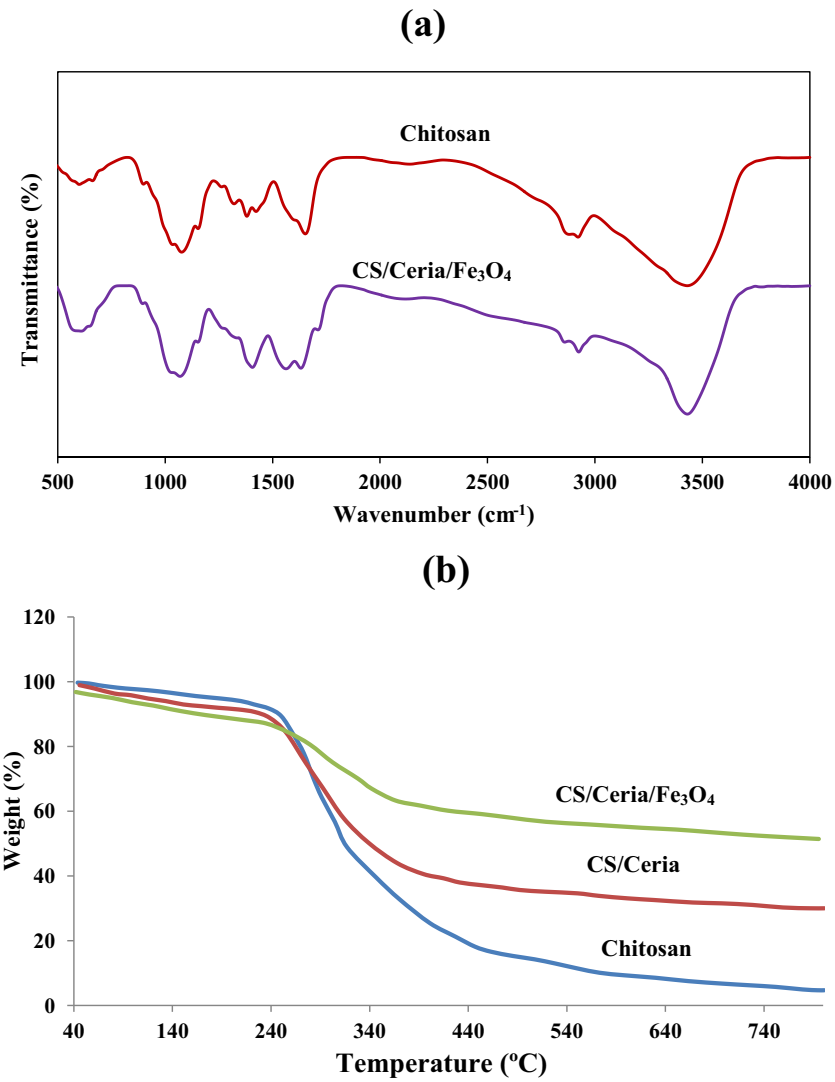

Fig. 3 **a** FTIR analysis for the pure chitosan and CS/ceria/Fe_3O_4 nano-composite adsorbent. **b** TGA curves for pure chitosan, chitosan/ceria and CS/ceria/Fe_3O_4 adsorbent

concentration of 200 mg/l for 100 min with an adsorbent dose of 0.5 g/l and pH 5.0 for Cr(VI) ions and pH 7.0 for Co(II) ions. The effect of CeO_2 contents on the adsorption of Cr(VI) and Co(II) ions is illustrated in Fig. 5a, b. As observed, the adsorption capacity of chitosan/CeO_2 increased significantly with the increase of CeO_2 contents nanoparticles from 0.25 to 1.0 g. The adsorption capacity of chitosan/CeO_2 with 0.25 and 1.0 g CeO_2 contents was found to be 52.7 and 114.3 mg/g for Cr(VI) ions and 46.7 and 96.5 mg/g for Co(II) ions. Further increase in CeO_2 contents (1.25 and 1.5 g) resulted in a decrease in adsorption capacity for Cr(VI) and Co(II) ions. This decrease can be due to the pore blockage by nanoparticle agglomeration leading to a reduction in surface area and active sites of adsorbent for the removal of Cr(VI) and Co(II) ions. Therefore, the optimum amount of CeO_2 content was found to be 1.0 g. The effect of Fe_3O_4 contents for the adsorption of Cr(VI) and Co(II) ions onto the chitosan/CeO_2/Fe_3O_4 nano-composite is shown in Fig. 5c, d. As observed, the adsorption capacity of chitosan/CeO_2/Fe_3O_4 nano-composite increased significantly with the increase of Fe_3O_4 contents nanoparticles from 0.4 to 1.2 g. It may be due to the surface area increase with the increase of Fe_3O_4 contents up to 1.2 g. Also, the presence of oxygen in the structure of Fe_3O_4 led to the increase of interaction between oxygen electron and metal ions. Further increase in Fe_3O_4 contents (1.4 g) led to a decrease in adsorption capacity for Cr(VI) and Co(II) ions due to the instability and agglomeration of Fe_3O_4 and reduction of surface area. Consequently, the optimum amounts of CeO_2 and Fe_3O_4 contents were found to be 1.0 and 1.2 g in the structure of chitosan/ceria/Fe_3O_4 nano-composite adsorbent and it was selected for the next adsorption experiments.

Effect of initial pH on Cr(VI) and Co(II) adsorption

The effect of initial pH of solution on the adsorption capacity of chitosan/CeO_2/Fe_3O_4 nano-composite adsorbent for Cr(VI) and Co(II) ions is indicated in Fig. 6a. The surface properties of the chitosan/CeO_2/Fe_3O_4 adsorbent are the most important factor due to the various species of chromium and cobalt ions in

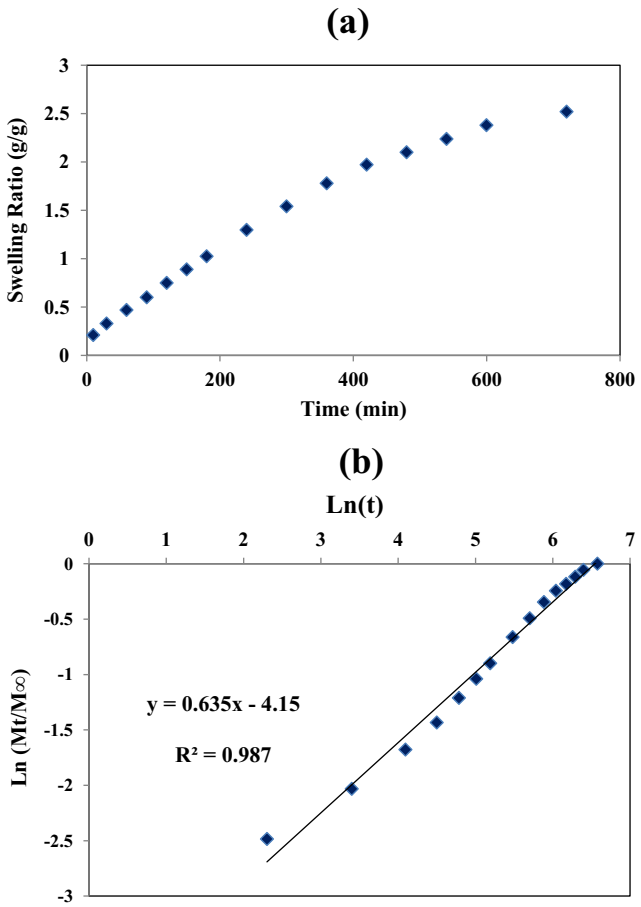

Fig. 4 **a** The swelling behavior of CS/Ceria/Fe_3O_4 nano-composite adsorbent. **b** the straight line of Ln(M_t/M_∞) versus Lnt

aqueous environment. Figure 6b shows the plot of final pH of solution versus initial pH of solution to determine the pH_{PZC}. The pH_{pzc} value of chitosan/ceria/Fe_3O_4 nano-composite was 6.8. As shown in Fig. 6a, the adsorption capacity decreased slowly with the increase of initial pH from 3.0 to 6.0 and then decreased significantly from pH 6.0 to 8.0. The corresponding mechanism can be explained by the chromium solution chemistry and the surface functional groups such as –OH and $–NH_2$ groups. There are five main chromium species containing H_2CrO_4, $HCrO_4$, CrO_4^{2} , HCr_2O_7 , and Cr_2O_7 in the acidic solution. At low pH, the protonation of $–NH_2$ groups to $–NH_3^+$ was easier according to Eq. (4). The point of zero charge confirmed the positive charge of the nano-composite surface at $pH < pH_{pzc}$. On the other hand, the competition of negative species of Cr(VI) with OH^- for occupancy of the active sites was lower at lower pH. Therefore, negatively charged Cr(VI) were attracted strongly on the positive surface of chitosan/ceria/Fe_3O_4 adsorbent at very low pH.

At higher pH, hydroxyl ions increased and the competition of chromium species with hydroxyl ions led to a decrease in adsorption capacity of chitosan/ceria/Fe_3O_4 nano-composite. Also, at $pH > pH_{pzc}$, the nano-composite was negatively charged resulting in an electrostatic repulsion between Cr(VI) anions and active sites of adsorbent. It was cleared that the reduction of adsorption capacity was obvious at around the pH_{PZC} due to the change of surface charge from positive to negative. A similar result was observed by Zhong et al. (2013). In the case of Co(II) (Fig. 6a), the adsorption capacity increased slowly with the increase of initial pH from 3.0 to 6.0 and then increased significantly from pH 6.0 to 8.0 and finally decreased from 8.0 to 9.0. The main cobalt species is Co(II) cation in the solution; therefore, the negative surface charge is needed to remove them from aqueous solutions (Wang et al. 2011). At very low pH, the competition of Co(II) with H^+ resulted in a lower adsorption capacity. In other words, the surface of adsorbent was positively charged ($pH < pH_{PZC}$) and an electrostatic repulsion between positive charge and Co(II) ions led to a decrease in adsorption capacity. At higher pH, hydroxyl ions increased significantly leading to the creation of negatively charged surface active sites of the chitosan/ceria/Fe_3O_4 through hydrogen bonds according to Eq. (5). Therefore, negatively charged surface active sites strongly attracted the cobalt species and increased the adsorption capacity. The abrupt increment of the adsorption capacity at around pH_{PZC} can be due to the change of adsorbent surface charge. At $pH > 8.0$, precipitation usually occurred and the hydroxyl complexes were formed which was the main reason for deterioration of the adsorbent leading to a reduction in adsorption capacity for Co(II) ions. Similar results were observed by Wang et al. (2011).

$$\text{Adsobent surface-}NH_2 + H^+ \Leftrightarrow –NH_3^+ \quad (4)$$

$$\text{Adsobent surface-}NH_2 + OH^- \Leftrightarrow \text{Adsobent surface-}NH_2 \ldots OH^- \quad (5)$$

Influence of contact time and kinetic models

The adsorption rate of Cr(VI) and Co(II) ions onto the chitosan/ceria/Fe_3O_4 nano-composite adsorbent was studied as a function of contact time in the range of 0–100 min for the initial concentration of 200 mg/l, adsorbent dosage of 0.5 g/l, and temperature of 25 °C with optimum pH values of 3.0 and 8.0 for Cr(VI) and Co(II), respectively. The results are indicated in Fig. 7. As observed, a rapid adsorption occurred during the first 45 min for both metal ions because all active sites of the nano-composite surface were vacant at the beginning of process and then the rate of adsorption became slower due to the saturation of active sites. For Cr(VI) and Co(II) ions, almost 90% of adsorption capacity was obtained within 45 min. Finally, the equilibrium contact time was found to be 100 min for both metal ions.

To understand the adsorption mechanism, four nonlinear kinetic models including double exponential, pseudo-first-order, pseudo-second-order, and Weber-Morris (intra-particle diffusion) models were applied. These nonlinear kinetic models are described by the following equations (Du et al. 2012; Talebi et al. 2017):

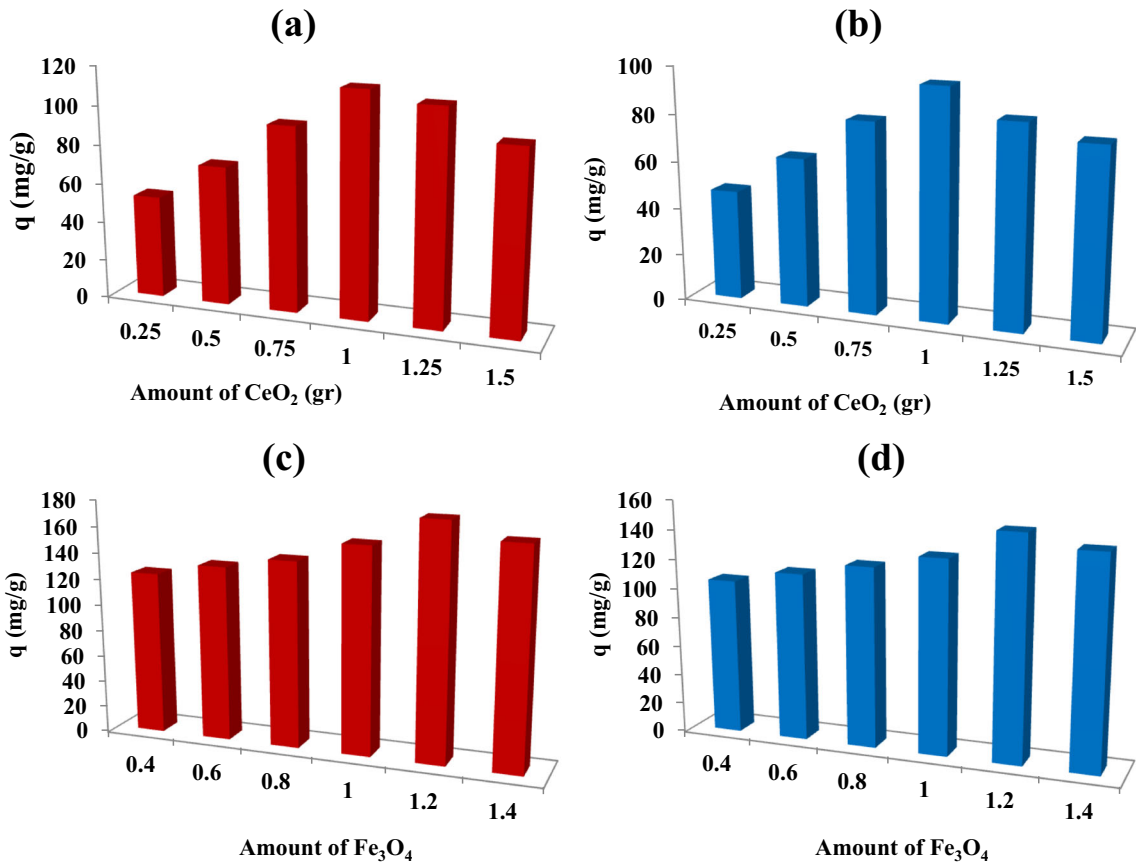

Fig. 5 Effect of ceria contents in the structure of chitosan for **a** Cr(VI) and **b** Co(II) adsorption and the effect of Fe_3O_4 contents in the structure of CS/Ceria adsorbent for **c** Cr(VI) and **d** Co(II) adsorption (at temperature of 25 °C, initial concentration of 200 mg/l, pH 5 for Cr(VI) and pH 7 for Co(II) ions, contact time of 100 min with an adsorbent dosage of 0.5 g/l)

$$\text{Pseudo-first-order}: q_t = q_e(1-\exp(-k_1 t)) \tag{6}$$

$$\text{Pseudo-second-order}: q_t = \frac{k_2 {q_e}^2 t}{1 + k_2 q_e t} \tag{7}$$

$$\text{Double exponential}: q_t = q_e - \frac{D_1}{m_{ads}}\exp(-k_{D1}t) - \frac{D_2}{m_{ads}}\exp(-k_{D2}t) \tag{8}$$

$$\text{Weber-Morris}: q_t = k_p\, t^{0.5} + C \tag{9}$$

where q_t and q_e (mmol/g) denote adsorption capacity of nano-composite adsorbents at time t and equilibrium time, respectively; k_1 (min^{-1}) represents the pseudo-first-order rate constant; k_2 (g mmol^{-1} min^{-1}) is the pseudo-second-order rate constant, respectively; D_1 and D_2 (g/l) are the rapid and slow rate constants, respectively; k_{D1} and k_{D2} (min^{-1}) represent the rapid and slow mass transfer coefficients, respectively; m_{ads} (g/l) represents the concentration of chitosan/ceria/Fe_3O_4 nano-composite adsorbent; C (mg/g) is a constant relating to the boundary layer thickness; and k_p (mg g^{-1} $\text{min}^{-0.5}$) shows the rate constant of intra-particle diffusion model. Diffusion of the metal ions to the active sites of adsorbent is the rate-limiting adsorption step in pseudo-first-order model, while the adsorption is controlled by chemisorption in pseudo-second-order model (Xu et al. 2017). Weber-Morris kinetic model represents that intra-particle diffusion controlled the adsorption process (Xu et al. 2017). When intra-particle diffusion only acts as the rate-limiting step, C value in Eq. (9) is close to zero and the line of q_t versus $t^{0.5}$ passes through the origin, approximately (Talebi et al. 2017). To understand a better curve fitting, the correlation coefficient (R^2) and the residual root mean square errors (RMSE) of kinetic models were applied. Higher R^2 and smaller RMSE displayed a better consistency of the experimental data with the models. RMSE was calculated as follows (Abbasizadeh et al. 2013):

$$\text{RMSE} = \sqrt{\left(\frac{1}{n-2}\right)\sum_{i=1}^{n}\left(q_{i,exp} - q_{i,cal}\right)^2} \tag{10}$$

where $q_{i,cal}$ and $q_{i,exp}$ (mmol/g) denote the adsorption capacity of calculated and the experimental values, respectively, and n is the number of data points.

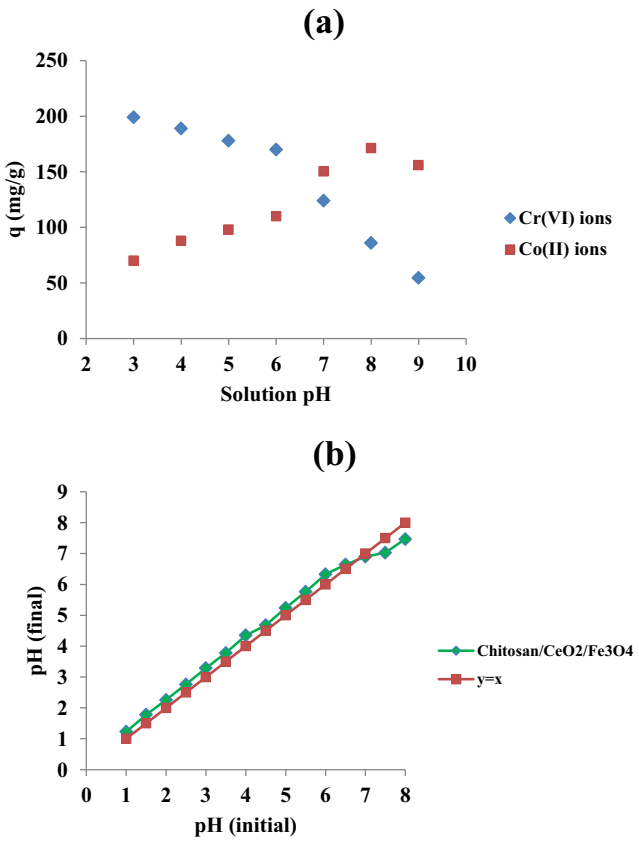

Fig. 6 **a** Effect of initial solution pH on Cr(VI) and Co(II) adsorption onto the CS/ceria/Fe_3O_4 nano-composite adsorbent (at temperature of 25 °C, initial concentration of 200 mg/l, contact time of 100 min with an adsorbent dosage of 0.5 g/l) and **b** determination of point of zero charge (pH_{pzc}) of CS/Ceria/Fe_3O_4 nano-composite adsorbent

In this research, the kinetic parameters were determined using simulation of kinetic data by the MATLAB software and the results are given in Table 2. As observed, R^2 (> 0.897) and RMSE (< 11.81) values for Weber-Morris kinetic model revealed that the adsorption process was not solely controlled by intra-particle diffusion and this model may have included several steps such as external surface adsorption and diffusion of Cr(VI) and Co(II) ions into the chitosan/ceria/Fe_3O_4 nano-composite pores. The values of R^2 and RMSE confirmed that the pseudo-second-order model showed a better curve fitting compared to pseudo-first-order model. This showed that the adsorption was controlled by chemisorption. Among all kinetic models, the highest R^2 (> 0.992) and the lowest RMSE (< 4.39) were found for double exponential kinetic model. This model suggested that the adsorption process included an initial rapid phase corresponding to the adsorption of Cr(VI) and Co(II) ions onto the external surface of chitosan/ceria/Fe_3O_4 nano-composite and a slow phase corresponding to the adsorption of metal ions on the interior surface of chitosan/ceria/Fe_3O_4 nano-composite adsorbent.

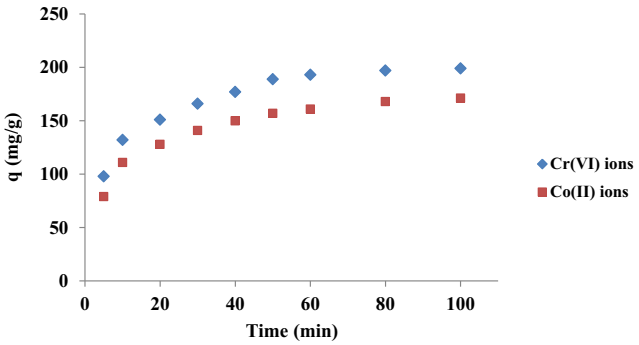

Fig. 7 The adsorption rate of Cr(VI) and Co(II) ions onto the CS/Ceria/Fe3O4 nano-composite adsorbent as a function of contact time (at temperature of 25 °C, initial concentration of 200 mg/l, with optimum pH 3.0 for Cr(VI) and pH 8.0 for Co(II) ions, contact time of 100 min with an adsorbent dosage of 0.5 g/l)

Effect of initial concentration and adsorption isotherms

Effect of initial concentration of Cr(VI) and Co(II) ions on the adsorption capacity of chitosan/ceria/Fe_3O_4 nano-composite adsorbent was investigated at 25 °C, contact time of 100 min, and adsorbent dosage of 0.5 g/l with an optimum pH values of 3.0 and 8.0 for Cr(VI) and Co(II), respectively. Figure 8 reveals a sharp increase in adsorption capacity at low initial concentration region because the available active sites of chitosan/ceria/Fe_3O_4 nano-composite adsorbent were sufficient to react with the both ions. With further increase in initial Cr(VI) and Co(II) concentrations, the adsorption capacity increased slowly because the active sites of adsorbent trended to saturate by Cr(VI) and Co(II) ions. The higher adsorption capacity at higher initial metal concentrations can be due to a greater driving force to overcome mass transfer resistances between the nano-composite adsorbent and the aqueous phase (Hallaji et al. 2015).

To study the interactions between the metal ions and adsorbent, three isotherms including Freundlich, Langmuir, and Dubinin–Radushkevich (D-R) were applied. A mathematical approach was used to simulate the adsorption behavior using MATLAB software. These isotherm models were explained briefly. The chemisorption and a monolayer adsorption onto the homogenous adsorbent surfaces are assumed by the Langmuir isotherm model (Ren et al. 2016). The nonlinear Langmuir model is expressed as follows (Liu et al. 2015):

$$q_e = \frac{q_m K_L C_e}{1 + K_L C_e} \tag{11}$$

where q_m (mg/g) represents the maximum adsorption capacity of adsorbents, k_L (l/mg) is the rate constant of Langmuir model corresponding to the adsorption energy or net enthalpy, and C_e (mg/l) shows the equilibrium

Table 2 Kinetic parameters for the Cr(VI) and Co(II) adsorption onto the CS/ceria/Fe_3O_4 nano-composite adsorbent

Metal	q_{exp} (mg/g)	Pseudo-first-order model						
		K_1 (min^{-1})		q (mg/g)	RMSE		R^2	
Cr(VI)	199.1	0.1174		187.0	12.87		0.877	
Co(II)	171.3	0.1118		158.7	10.53		0.894	
		Pseudo-second-order model						
		$K_2 \times 10^4$ (g/mg min)		q (mg/g)	RMSE		R^2	
Cr(VI)	199.1	7.68		209.0	5.45		0.978	
Co(II)	171.3	8.37		178.4	4.48		0.984	
		Double exponential kinetic model						
		D_1 (g/l)	K_{D1} (min^{-1})	D_2 (g/l)	K_{D2} (min^{-1})	q (mg/g)	RMSE	R^2
Cr(VI)	199.1	55.08	0.0459	3010	1.266	197.1	4.39	0.992
Co(II)	171.3	43.66	0.0315	1894	1.042	174.8	0.475	0.999
		Weber-Morris model						
		K_p (mg/(g min))		C (mg/g)	RMSE		R^2	
Cr(VI)	199.1	12.56		89.51	11.81		0.897	
Co(II)	171.3	11.10		72.35	9.99		0.904	

concentration of metal ions. A dimensionless separation factor (R_L) was used to examine the types of isotherm which is calculated as follows (Abbasizadeh et al. 2014):

$$R_L = \frac{1}{1 + K_L C_0} \tag{12}$$

where C_0 is the highest initial Cr(VI) and Co(II) concentrations. The type of isotherm is irreversible for $R_L = 0$, linear for $R_L = 1$, favorable for $0 < R_L < 1$, and unfavorable for $R_L > 1$.

The Freundlich isotherm is an empirical equation that was applied to interpret the multilayer adsorption onto the heterogeneous surface. The Freundlich model is expressed as follows (Ahmad et al. 2017; Sheshdeh et al. 2014):

$$q_e = K_F C_e^{1/n} \tag{13}$$

where K_F ((mg/g)/(l/mg)$^{1/n}$) shows the adsorption capacity and n represents the heterogeneity factor corresponding to the adsorption intensity. The adsorption is feasible for $n > 1$ (El-Reash et al. 2016).

The D-R isotherm was applied to specify the chemical or physical type of adsorption. It is defined as follows (Ji et al. 2012):

$$q_e = q_{DR}\exp\left(-B_{DR}\varepsilon^2\right), \quad \varepsilon = RT\ln\left(1 + \frac{1}{C_e}\right) \tag{14}$$

where q_{DR} shows the theoretical saturation capacity, ε is the Polanyi potential, B_{DR} (mol^2/J^2) represents the activity coefficient corresponding to the mean free energy of adsorption, and $T(K)$ is the absolute temperature. The mean free energy of adsorption (E (kJ/mol)) can be estimated as follows (Abbasizadeh et al. 2014):

$$E = \frac{1}{\sqrt{2B_{DR}}} \tag{15}$$

The physical adsorption has E values in the range of 1–8 kJ/mol, while chemical adsorption is a dominant mechanism for $8 < E$ (kJ/mol) < 16 (Abbasizadeh et al. 2014).

Parameters of isotherm models are given in Table 3. By comparing the R^2 values for all isotherms, the experimental data were well fitted with the Langmuir isotherm model ($R^2 >$ 0.993). Furthermore, q_m of chitosan/ceria/Fe_3O_4 nano-

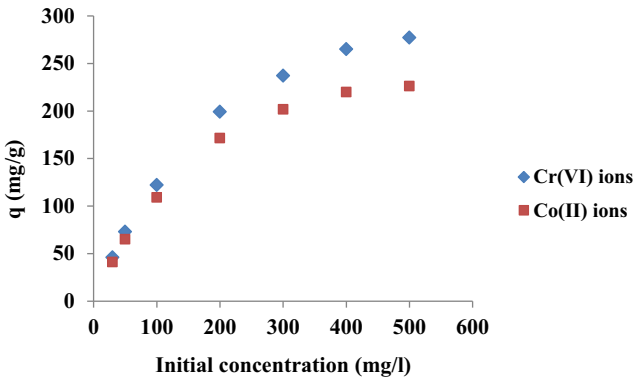

Fig. 8 Effect of initial Cr(VI) and Co(II) concentrations on the adsorption capacity of CS/Ceria/Fe_3O_4 nano-composite adsorbent in the single system (at temperature of 25 °C, contact time of 100 min, adsorbent dosage of 0.5 g/l with an optimum pH values of 3.0 and 8.0 for Cr(VI) and Co(II), respectively)

composite adsorbent was found to be 315.4 and 260.6 mg/g for Cr(VI) and Co(II) ions, respectively. The values of R_L were in the range of 0–1 indicating the favorable adsorption. The favorable adsorption was confirmed by the n (greater than one) values obtained from Freundlich isotherm model. The values of E obtained from D-R model were found to be 1–8 kJ/mol, showing the physical adsorption for both Cr(VI) and Co(II) ions.

Thermodynamic parameters

To investigate the mechanism of energy-dependent in heavy metal adsorption, the medium temperature is a key parameter. The Cr(VI) and Co(II) adsorption onto the chitosan/ceria/Fe_3O_4 nano-composite was studied at various temperatures (25–45 °C) to estimate the thermodynamic parameters. The Gibbs energy change ($\Delta G°$), enthalpy change ($\Delta H°$), and entropy change ($\Delta S°$) were determined by the following equations (Sheng et al. 2010; Talebi et al. 2017):

$$\Delta G^{\circ} = -RT\ln K_d \tag{16}$$

$$\ln(K_d) = \frac{\Delta S^{\circ}}{R} - \frac{\Delta H^{\circ}}{R} \times \frac{1}{T} \tag{17}$$

where $T(K)$ represents the absolute temperature and K_d is the thermodynamic equilibrium constant which is calculated using $k_d = q_e/C_e$ (Sheng et al. 2010). The $\Delta S°$ and $\Delta H°$ parameters were determined from intercept and slope of the plot of $\mathrm{Ln}(K_c)$ versus $1/T$, respectively. Table 4 reveals all the thermodynamic parameters. As observed, the signs of $\Delta G°$ values for both Cr(VI) and Co(II) ions were negative indicating the feasibility and spontaneity of adsorption process. The $\Delta G°$ values were obtained in the range of 0 to − 20 kJ/mol showing a dominant physical adsorption and weak chemisorption of Cr(VI) and Co(II) ions onto the nano-composite adsorbent. Similar results were obtained by others (Liu et al. 2005).

Table 3 Isotherm parameters for the Cr(VI) and Co(II) adsorption onto the CS/ceria/Fe_3O_4 nano-composite adsorbent

Metal	Langmuir isotherm			
	q_m (mg/g)	K_L (L/mg)	R_L	R^2
Cr(VI)	315.4	0.0180	0.100	0.993
Co(II)	260.6	0.172	0.104	0.998
	Freundlich isotherm			
	K_F (mg/g)	n		R^2
Cr(VI)	29.37	2.554		0.971
Co(II)	24.51	2.594		0.964
	Dubinin–Radushkevich isotherm			
	q_{DR} (mmol/g)	B_{DR} (mol^2/J^2) × 10^7	E (kJ/mol)	R^2
Cr(VI)	4.847	1.048	2.184	0.911
Co(II)	3.601	1.074	2.157	0.935

More feasible Cr(VI) and Co(II) adsorptions onto the chitosan/ceria/Fe_3O_4 adsorbent were obtained at a lower temperature because $\Delta G°$ values decreased with the increase of temperature from 25 to 45 °C. The negative values of $\Delta H°$ suggested that the adsorption of both Cr(VI) and Co(II) ions was an endothermic process. This indicated that the adsorption capability of Cr(VI) and Co(II) ions onto chitosan/ceria/Fe_3O_4 nano-composite adsorbent decreased with the increase of temperature from 25 to 45 °C. The $\Delta S°$ values showed that the randomness of metal ions at the adsorbent–liquid interface during the adsorption process decreased with increasing the temperature.

Regeneration ability of chitosan/ceria/Fe_3O_4 nano-composite adsorbent

The regeneration tests were performed using 0.1 M NaOH and 0.1 M HNO_3 as stripping agents in a batch system for four cycles of adsorption-desorption. Table 5 indicates the results of regeneration tests. As observed, the adsorption capacity of chitosan/ceria/Fe_3O_4 nano-composite adsorbent for Co(II) ions decreased from 171.3 to 114.4 using 0.1 M NaOH and 171.3 to 158.6 using 0.1 M HNO_3. For desorption of Co(II) ions from the adsorbent surface, the best performance was found for 0.1 M HNO_3 because the reduction percentage of adsorption capacity was only 7.4% after four cycles. For Cr(VI) ions, the best stripping agent was 0.1 M NaOH because the adsorption capacity indicated a little decrease (only 8.9% after four cycles of adsorption-desorption). Therefore, the results showed that the chitosan/ceria/Fe_3O_4 nano-composite adsorbent with an appropriate striping agent can be reused frequently in adsorption process.

Table 4 Thermodynamic parameters for the adsorption of Cr(VI) and Co(II) ions onto the CS/ceria/Fe_3O_4 nano-composite adsorbent

Parameter	Temperature	Metal ions	
		Cr(VI)	Co(II)
K_d	25 °C	1.982	1.498
	30 °C	1.883	1.419
	35 °C	1.809	1.347
	40 °C	1.704	1.292
	45 °C	1.630	1.252
$G°$ (kJ/mol) Δ	25 °C	− 1695.0	− 1001.3
	30 °C	− 1594.9	− 881.2
	35 °C	− 1518.7	− 763.3
	40 °C	− 1386.5	− 667.05
	45 °C	− 1291.4	− 594.3
$H°$ (J/mol)Δ		− 7745.2	− 7138.9
$S°$ (J/mol K)Δ		− 20.28	− 20.64

Table 5 Regeneration of CS/ceria/Fe_3O_4 nano-composite adsorbent using two different stripping agents

Stripping agents	Metal	q (mg/g) before esorption	q (mg/g) for 4 cycles			
			1	2	3	4
NaOH	Cr(VI)	199.1	194.2	191.0	184.6	181.3
	Co(II)	171.3	133.2	126.0	121.2	114.4
HNO_3	Cr(VI)	199.1	165.8	154.7	149.1	142.0
	Co(II)	171.3	168.2	164.0	161.9	158.6

Simultaneous adsorption of Cr(VI) and Co(II) ions

The influence of Cr(VI) and Co(II) coexisting on the adsorption capacity of nano-composite was investigated in binary systems. In a binary system, the effect of initial Co(II) concentration on the adsorption capacity for Cr(VI) ions was evaluated by varying the initial Cr(VI) concentration from 0 to 300 mg/l, while the initial concentration of Co(II) was fixed at 0, 30, 50, 100, 200, and 300 mg/l at pH 3.0 and 8.0. The experimental results in the absence and presence of Co(II) ions are revealed in Fig. 9a, c. As observed, the adsorption capacity of chitosan/ceria/Fe_3O_4 nano-composite for Cr(VI) ions in the presence of Co(II) ions was lower than that in the absence of Co(II) ions at two pH values. It showed that there was a competition between Cr(VI) and Co(II) ions to occupy the active sites of nano-composite adsorbent. It was clearly observed that the adsorption capacity for Cr(VI) ions increased with increasing the initial Cr(VI) concentration in both single and binary systems. On the other hand, the adsorption capacity for Cr(VI) ions decreased with increasing the Co(II) ions as inhibitor ions. At 200 mg/l of initial concentration of Cr(VI), in the absence of Co(II) ions and in the presence of 200 mg/l of initial Co(II) concentration, the adsorption capacities for Cr(VI) ions were found to be 199.1 and 168.0 mg/g at pH 3.0 and 86.0 and 42.0 mg/g at pH 8.0, respectively. Furthermore, Fig. 9b, d indicates the influence of initial Cr(VI) concentration as inhibitor ions on adsorption capacity for Co(II) ions at pH 3.0 and 8.0. As shown, similar adsorption

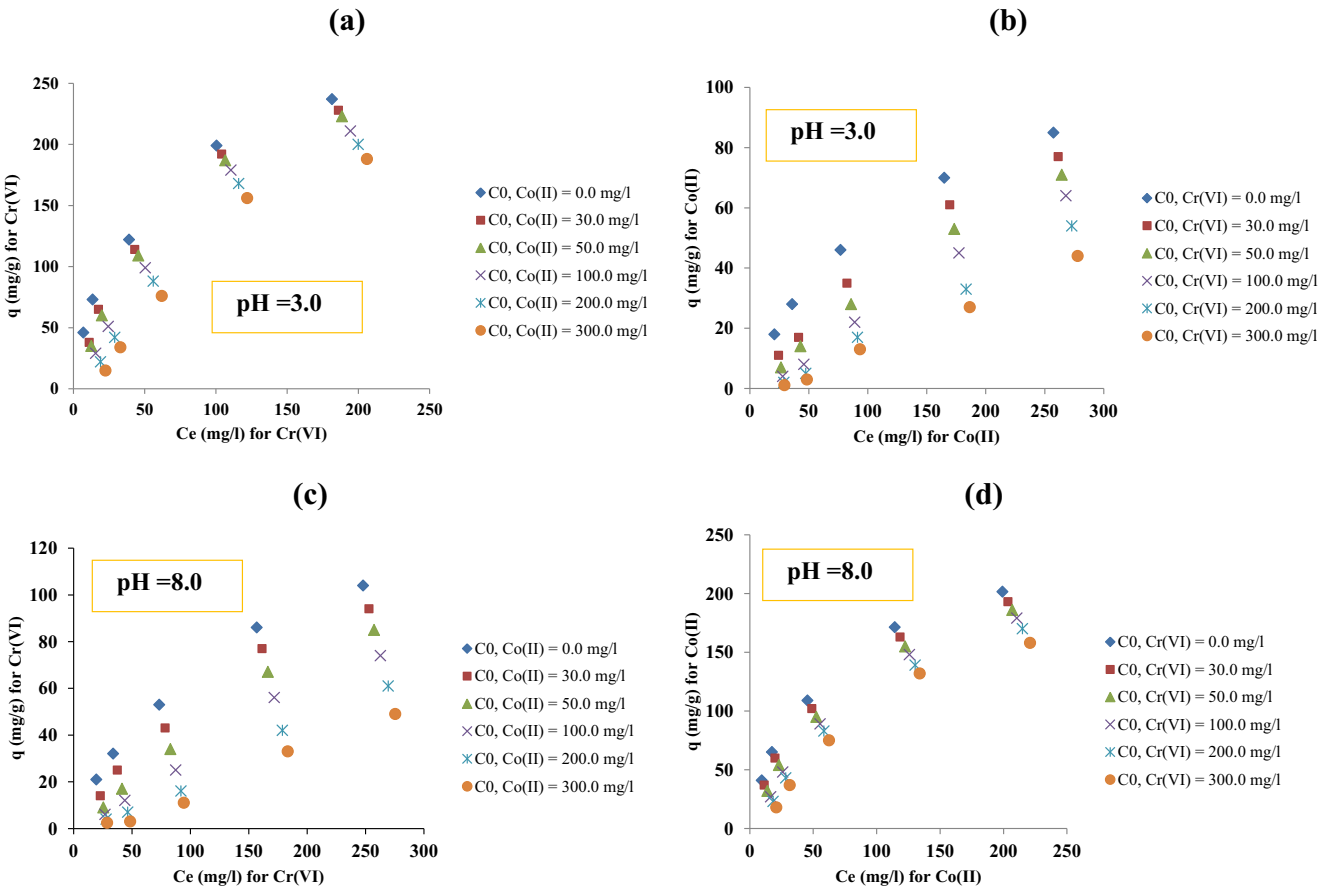

Fig. 9 **a** Effect of initial Co(II) concentration on the adsorption capacity for Cr(VI) ions at pH 3.0. **b** Effect of initial Cr(VI) concentration on the adsorption capacity for Co(II) ions at pH 3.0. **c** Effect of initial Co(II) concentration on the adsorption capacity for Cr(VI) ions at pH 8.0. **d** Effect of initial Cr(VI) concentration on the adsorption capacity for Co(II) ions at pH 8.0 in the binary systems

patterns were obtained in the single Co(II) and binary Cr(VI)-Co(II) systems. The selectivity of chitosan/ceria/Fe_3O_4 nano-composite for Co(II) ions increased with decreasing the initial Cr(VI) concentration in the binary system. In the absence of Cr(VI) ions, the adsorption capacity of nano-composite for Co(II) ion was 70.0 and 171.3 mg/g with the initial Co(II) concentration of 200 mg/l at pH 3.0 and 8.0, respectively. When the concentration of inhibitor Cr(VI) ions was kept at 200 mg/l, the adsorption capacity for Co(II) ion decreased to 33.0 and 139.0 mg/g at pH 3.0 and 8.0, respectively. Comparison of Fig. 9a with b revealed that the inhibitory influence of Cr(VI) ions on the Co(II) adsorption was greater than the inhibitory influence of Co(II) ion on the Cr(VI) adsorption at pH 3.0, while the influence of inhibitor Co(II) ions on the Cr(VI) adsorption was greater than the influence of Cr(VI) ions on the Co(II) adsorption at pH 8.0 by comparison of Fig. 9c with d. The adsorption equilibrium data in the binary systems showed that the combined influences of Cr(VI) and Co(II) ions appeared to be antagonistic.

Conclusion

In this study, a novel CS/ceria/Fe_3O_4 nano-composite adsorbent was prepared for the removal of Cr(VI) and Co(II) ions from single and binary systems. The nano-composite adsorbents were characterized by FESEM, XRD, BET, FTIR, and TGA analyses. The TGA results indicated that the thermal stability of CS/ceria/Fe_3O_4 nano-composite was greater than that of pure chitosan. Also, the characterization results showed that the chitosan surface was successfully coated with CeO_2 and Fe_3O_4 nanoparticles. The highest surface area and average pore volume were found to be 118.7 m^2/g and 0.0603 cm^3/g for CS/ceria/Fe_3O_4 with 1.0 g of ceria and 1.2 g of Fe_3O_4 nanoparticles. The swelling kinetic behavior of CS/ceria/Fe_3O_4 nano-composite followed non-Fickian mechanism. The equilibrium data were best fitted by the Langmuir model. The q_{max} of nano-composite for Cr(VI) and Co(II) ions obtained from Langmuir isotherm model were 315.4 and 260.6 mg/g, respectively. Among kinetic models, the double exponential model showed the best correlation with the experimental data for both Cr(VI) and Co(II) ions. The thermodynamic parameters showed that the adsorption process was feasible and spontaneous for both Cr(VI) and Co(II) ions with a negative $\Delta G°$ value. Also, a negative value of $\Delta G°$ revealed the exothermic nature of Cr(VI) and Co(II) adsorption. The regeneration experiments after four cycles of adsorption-desorption confirmed that CS/ceria/Fe_3O_4 adsorbent could be used repeatedly for the removal of Cr(VI) and Co(II) ions from aqueous solution. The adsorption equilibrium data in the binary systems showed that the Co(II) ions had an inhibitor effect on the adsorption of Cr(VI) ions.

References

Abbasizadeh S, Keshtkar AR, Mousavian MA (2013) Preparation of a novel electrospun polyvinyl alcohol/titanium oxide nanofiber adsorbent modified with mercapto groups for uranium(VI) and thorium(IV) removal from aqueous solution. Chem Eng J 220: 161–171

Abbasizadeh S, Keshtkar AR, Mousavian MA (2014) Sorption of heavy metal ions from aqueous solution by a novel cast PVA/TiO_2 nanohybrid adsorbent functionalized with amine groups. J Ind Eng Chem 20:1656–1664

Ahmad NF, Kamboh MA, Nodeh HR, Halim SNBA, Mohamad S (2017) Synthesis of piperazine functionalized magnetic sporopollenin: a new organic-inorganic hybrid material for the removal of lead(II) and arsenic(III) from aqueous solution. Environ Sci Pollut Res 24: 21846–21858

Ahmadpour A, Tahmasbi M, Bastami TR, Besharati JA (2009) Rapid removal of cobalt ion from aqueous solutions by almond green hull. J Hazard Mater 166:925–930

Bai Y, Bartkiewicz B (2009) Removal of cadmium from wastewater using ion exchange resin Amberjet 1200H columns. Polish J Enviro Stud 18:1191–1195

Becker F, Rodríguez D, Schwab M (2012) Magnetic removal of cobalt from waste water by ferrite co-precipitation. Procedia Mater Sci 1: 644–650

Bhatnagar A, Sillanpää M (2009) Applications of chitin- and chitosan-derivatives for the detoxification of water and wastewater—a short review. Adv Colloid Interf Sci 152:26–38

Cao C, Xiao L, Chen C, Shi X, Cao Q, Gao L (2014) In situ preparation of magnetic Fe_3O_4/chitosan nanoparticles via a novel reduction–precipitation method and their application in adsorption of reactive azo dye. Powder Technol 260:90–97

Chen L-F, Liang H-W, Lu Y, Cui C-H, Yu S-H (2011) Synthesis of an attapulgite clay@ carbon nanocomposite adsorbent by a hydrothermal carbonization process and their application in the removal of toxic metal ions from water. Langmuir 27:8998–9004

Coll M, Fortuny A, Kedari C, Sastre A (2012) Studies on the extraction of Co(II) and Ni(II) from aqueous chloride solutions using Primene JMT-Cyanex272 ionic liquid extractant. Hydrometallurgy 125:24–28

Du G, Li Z, Liao L, Hanson R, Leick S, Hoeppner N, Jiang W-T (2012) Cr(VI) retention and transport through Fe (III)-coated natural zeolite. J Hazard Mater 221:118–123

El-Reash YA, Abdelghany A, Elrazak AA (2016) Removal and separation of Cu(II) from aqueous solutions using nano-silver chitosan/polyacrylamide membranes. Inter J Biol Macromol 86:789–798

Ferfera-Harrar H, Dairi N (2014) Green nanocomposite films based on cellulose acetate and biopolymer-modified nanoclays: studies on morphology and properties. Iranian Polym J 23:917–931

Hallaji H, Keshtkar AR, Moosavian MA (2015) A novel electrospun PVA/ZnO nanofiber adsorbent for U(VI), Cu(II) and Ni(II) removal from aqueous solution. J Taiwan Inst Chem Eng 46:109–118

Ji F, Li C, Tang B, Xu J, Lu G, Liu P (2012) Preparation of cellulose acetate/zeolite composite fiber and its adsorption behavior for heavy metal ions in aqueous solution. Chem Eng J 209:325–333

Kim S, Chu KH, Al-Hamadani YA, Park CM, Jang M, Kim D-H, Yu M, Heo J, Yoon Y (2017) Removal of contaminants of emerging concern by membranes in water and wastewater: a review. Chem Eng J 335:896–914

Kim SJ, Lee KJ, Kim IY, Lee YM, Kim SI (2003) Swelling kinetics of modified poly (vinyl alcohol) hydrogels. J Appl Polym Sci 90: 3310–3313

Li X, Gao X, Ai L, Jiang J (2015) Mechanistic insight into the interaction and adsorption of Cr(VI) with zeolitic imidazolate framework-67 microcrystals from aqueous solution. Chem Eng J 274:238–246

Liu C-C, Kuang-Wang M, Li Y-S (2005) Removal of nickel from aqueous solution using wine processing waste sludge. Ind Eng Chem Res 44:1438–1445

Liu J-F, Z-s Z, G-b J (2008) Coating Fe_3O_4 magnetic nanoparticles with humic acid for high efficient removal of heavy metals in water. Environ Sci Technol 42:6949–6954

Liu W, Zhang J, Jin Y, Zhao X, Cai Z (2015) Adsorption of Pb(II), Cd(II) and Zn(II) by extracellular polymeric substances extracted from aerobic granular sludge: efficiency of protein. J Environ Chem Eng 3: 1223–1232

Mirbagheri S, Hosseini S (2005) Pilot plant investigation on petrochemical wastewater treatment for the removal of copper and chromium with the objective of reuse. Desalination 171:85–93

Petrella A, Spasiano D, Acquafredda P, De Vietro N, Ranieri E, Cosma P, Rizzi V, Petruzzelli V, Petruzzelli D (2018) Heavy metals retention (Pb(II), Cd(II), Ni(II)) from single and multimetal solutions by natural biosorbents from the olive oil milling operations. Process Saf Environ Protect 114:79–90

Polat H, Erdogan D (2007) Heavy metal removal from waste waters by ion flotation. J Hazard Mater 148:267–273

Prakash N, Sudha P, Renganathan N (2012) Copper and cadmium removal from synthetic industrial wastewater using chitosan and nylon 6. Environ Sci Pollut Res 19:2930–2941

Prakash N, Latha S, Sudha PN, Renganathan NG (2013) Influence of clay on the adsorption of heavy metals like copper and cadmium on chitosan. Environ Sci Pollut Res 20:925–938

Prakash N, Latha S, Sudha P, Renganathan N (2016) Kinetics of removal of chromium from wastewater using chitosan-based binary polymer blends. Synth React Inorg Met-Org Nano-Metal Chem 46:1310–1317

Ray PZ, Shipley HJ (2015) Inorganic nano-adsorbents for the removal of heavy metals and arsenic: a review. RSC Adv 5:29885–29907

Recillas S, Colón J, Casals E, González E, Puntes V, Sánchez A, Font X (2010) Chromium VI adsorption on cerium oxide nanoparticles and morphology changes during the process. J Hazard Mater 184:425–431

Ren H, Jiang J, Wu D, Gao Z, Sun Y, Luo C (2016) Selective adsorption of Pb(II) and Cr(VI) by surfactant-modified and unmodified natural zeolites: a comparative study on kinetics, equilibrium, and mechanism. Water Air Soil Pollut 227:101

Shen H, Pan S, Zhang Y, Huang X, Gong H (2012) A new insight on the adsorption mechanism of amino-functionalized nano-Fe_3O_4 magnetic polymers in Cu(II), Cr(VI) co-existing water system. Chem Eng J 183:180–191

Sheng G, Shao D, Ren X, Wang X, Li J, Chen Y, Wang X (2010) Kinetics and thermodynamics of adsorption of ionizable aromatic compounds from aqueous solutions by as-prepared and oxidized multiwalled carbon nanotubes. J Hazard Mater 178:505–516

Sheshdeh RK, Abbasizadeh S, Nikou MRK, Badii K, Sharafi MS (2014) Liquid phase adsorption kinetics and equilibrium of toluene by novel modified-diatomite. J Environ Health Sci Eng 12:148

Sirk KM, Saleh NB, Phenrat T, Kim H-J, Dufour B, Ok J, Golas PL, Matyjaszewski K, Lowry GV, Tilton RD (2009) Effect of adsorbed polyelectrolytes on nanoscale zero valent iron particle attachment to soil surface models. Environ Sci Technol 43:3803–3808

Sun J, Wang C, Zeng L, Xu P, Yang X, Chen J, Xing X, Jin Q, Yu R (2016) Controllable assembly of CeO2 micro/nanospheres with adjustable size and their application in Cr(VI) adsorption. Mater Res Bulletin 75:110–114

Sureshkumar V, Daniel SK, Ruckmani K, Sivakumar M (2016) Fabrication of chitosan–magnetite nanocomposite strip for chromium removal. Appl Nanosci 6:277–285

Taboada E, Cabrera G, Jimenez R, Cardenas G (2009) A kinetic study of the thermal degradation of chitosan-metal complexes. J Appl Polym Sci 114:2043–2052

Talebi M, Abbasizadeh S, Keshtkar AR (2017) Evaluation of single and simultaneous thorium and uranium sorption from water systems by an electrospun PVA/SA/PEO/HZSM5 nanofiber. Process Saf Environ Protect 109:340–356

Tehrani MM, Abbasizadeh S, Alamdari A, Mousavi SE (2017) Prediction of simultaneous sorption of copper (II), cobalt (II) and zinc (II) contaminants from water systems by a novel multi-functionalized zirconia nanofiber. Desalin Water Treat 62:403–417

Wang Q, Li J, Chen C, Ren X, Hu J, Wang X (2011) Removal of cobalt from aqueous solution by magnetic multiwalled carbon nanotube/iron oxide composites. Chem Eng J 174:126–133

Wang Y, Zhang Y, Hou C, Liu M (2016) Mussel-inspired synthesis of magnetic polydopamine–chitosan nanoparticles as biosorbent for dyes and metals removal. J Taiwan Inst Chem Eng 61:292–298

Xu Q, Wang Y, Jin L, Wang Y, Qin M (2017) Adsorption of Cu(II), Pb(II) and Cr(VI) from aqueous solutions using black wattle tannin-immobilized nanocellulose. J Hazard Mater 339:91–99

Yari S, Abbasizadeh S, Mousavi SE, Moghaddam MS, Moghaddam AZ (2015) Adsorption of Pb(II) and Cu(II) ions from aqueous solution by an electrospun CeO_2 nanofiber adsorbent functionalized with mercapto groups. Process Saf Environ Protect 94:159–171

Zhang S, Zhang Y, Bi G, Liu J, Wang Z, Xu Q, Xu H, Li X (2014) Mussel-inspired polydopamine biopolymer decorated with magnetic nanoparticles for multiple pollutants removal. J Hazard Mater 270:27–34

Zhong Q-Q, Yue Q-Y, Gao B-Y, Li Q, Xu X (2013) A novel amphoteric adsorbent derived from biomass materials: synthesis and adsorption for Cu(II)/Cr(VI) in single and binary systems. Chem Eng J 229:90–98

Zhu K, Duan Y, Wang F, Gao P, Jia H, Ma C, Wang C (2017) Silane-modified halloysite/Fe_3O_4 nanocomposites: simultaneous removal of Cr(VI) and Sb(V) and positive effects of Cr(VI) on Sb(V) adsorption. Chem Eng J 311:236–246